Hybrid Invariant Extended Kalman Filtering for Bipedal Robot Walking on Dynamic Rigid Surfaces ⋆

Yuan Gao * and **Yan Gu** *

* *Department of Mechanical Engineering, University of Massachusetts Lowell, Lowell, MA, U.S.A.*
(e-mail: Yuan_Gao@ student.uml.edu, Yan_Gu@uml.edu)

Abstract: This paper introduces a hybrid invariant extended Kalman filtering (HInEKF) method for a class of nonlinear hybrid dynamical systems with state-triggered jumps and group affine continuous-time subsystems. The method is derived based on the provable extension of the existing InEKF design for group affine systems without state-triggered jumps. Sufficient stability conditions are provided to guarantee the asymptotic error convergence for the hybrid system. Furthermore, the complete characterization of nonlinear jump maps whose associated error jump maps are identity on the matrix Lie group is provided along with the greatly simplified observer design for such systems. Simulation results of bipedal walking on a dynamic rigid surface (i.e., rigid surfaces that move in the inertial frame) validate the theoretical results. Comparative simulations demonstrate the effectiveness of the proposed HInEKF methodology over the existing salted extended Kalman filtering (SEKF) for hybrid systems with state-triggered jumps.

1. INTRODUCTION

Various critical real-world applications demand accurate, provably stable estimator designs for hybrid systems with state-triggered jumps. Such systems include legged robot locomotion systems, which have the potential to benefit a wide range of tasks such as delivery and carrier services and emergency response. Yet, state estimation for these systems remains a challenging problem mainly due to their complex dynamics that involve continuous-time subsystems and state-triggered jumps (e.g., sudden changes in a walking robot's suppot-foot positions at foot touchdowns). In particular, these jumps may cause sudden increases in the estimation errors, and their occurrence is state-dependent (Saccon et al. (2014); Iqbal et al. (2020, 2021)).

1.1 Related Work

Observer designs for *linear* hybrid systems with state-triggered jumps have been recently introduced to achieve provable error convergence (Bernard and Sanfelice (2018); Ríos et al. (2020)). Real-time observers for *nonlinear* hybrid dynamical systems with periodic solutions (e.g., legged locomotion systems) have been created to provably guarantee the error convergence based on the orbital stability conditions (Hamed et al. (2018)). Yet, this method cannot be used to estimate nonperiodic state trajectories of general nonlinear hybrid systems. To estimate general (periodic or nonperiodic) state trajectories, the Salted Extended Kalman Filter (SEKF) has been introduced (Kong et al. (2020)), which expands the extended Kalman filter (EKF) from systems without jumps to nonlinear hybrid dynamical systems. The key novelty of this approach is to propagate the estimated covariance matrix through the saltation matrix (Saccon et al. (2014)) at a jump event. Still, it suffers from the common disadvantage of the EKF in handling nonlinear systems; that is, the filter is built upon a system linearization whose accuracy cannot be controlled and thus adversely affects the gain computation (Barrau and Bonnabel (2017)). Thus, the SEKF cannot provably guarantee the error convergence for a deterministic nonlinear hybrid system.

For systems with invariant dynamics on Lie groups and without state-triggered jumps, invariant extended Kalman filters (InEKF) have been introduced (Barrau and Bonnabel (2017); de Ruiter and Forbes (2017)). Because the linearized error dynamics during the propagation step of filtering are independent from the group configuration, the InEKF is an asymptotic observer for deterministic group affine systems. Its guarantee on asymptotic error convergence is in sharp contract to the conventional EKF that cannot ensure such provable convergence. Recently, the InEKF has been applied and experimentally implemented for bipedal walking on stationary surfaces under the assumption that the jump events (i.e., foot touchdowns) are instantaneously detected (Hartley et al. (2020)). The InEKF achieves significant improvement in state estimation performance (e.g., convergence rate) over existing EKF-based methods (Bloesch et al. (2013); Bledt et al. (2018)). However, this method is created largely based on the continuous-time subsystem of the hybrid walking dynamics. In particular, the error convergence is not provably analyzed for the hybrid model of bipedal walking.

⋆ Research by Y. Gao and Y. Gu was supported in part by NSF under Grant no. CMMI-1934280. Corresponding author: Y. Gu.

1.2 Contributions

This study aims to introduce a provably convergent hybrid invariant extended Kalman filtering (HInEKF) approach for a class of *nonlinear* hybrid dynamical systems with state-triggered jumps under the assumption that the jumps are instantaneously detected. To our best knowledge, this is the first time that InEKF has been provably extended to explicitly address nonlinear hybrid systems with state-triggered jumps.

The main contributions of this study are: a) provably extending the InEKF method to a general class of *nonlinear* hybrid systems with state-triggered jumps under the assumption of instantaneous jump detection. b) Characterizing a class of hybrid dynamical systems whose deterministic error jump map on Lie groups is identity. Such systems enjoy the rare property for hybrid systems with state-triggered jumps that the error on Lie groups does not expand when the true state jumps. c) Validating the convergence of the proposed filter design through simulations of a new locomotion task of bipedal walking on nonstationary surfaces. d) Demonstrating through simulations the improved convergence performance of the proposed HInEKF over the existing SEKF for hybrid systems.

This paper is organized as follows. Section 2 explains a brief mathematical background on Lie groups. Section 3 presents the problem formulation. Section 4 introduces the proposed HInEKF algorithm for state-triggered jumps. Section 5 discusses the Lyapunov-based stability analysis of the proposed estimator. Section 6 provides the complete characterization of a particular class of hybrid dynamical systems whose estimation error jump maps under the HInEKF are identity. Section 7 reports the simulation setup and results that validate the proposed filter design. Section 8 gives the concluding remarks.

2. PRELIMINARIES

The matrix Lie group, denoted as $\mathcal{G}$, is a subset of $N \times N$ invertible square matrices possessing the following properties: $\mathbf{I}_N \in \mathcal{G}$; $\forall \mathbf{X} \in \mathcal{G}, \mathbf{X}^{-1} \in \mathcal{G}$; and $\forall \mathbf{X}_1, \mathbf{X}_2 \in \mathcal{G}, \mathbf{X}_1\mathbf{X}_2 \in \mathcal{G}$, where $\mathbf{I}_N$ is an $N \times N$ identity matrix. The associated Lie algebra $\mathfrak{g}$ with a dimension of $\dim\mathfrak{g}$ is a set of $N \times N$ square matrices. The linear operator $(\cdot)^\wedge$ maps any vector $\boldsymbol{\xi} \in \mathbb{R}^{\dim\mathfrak{g}}$ onto $\mathfrak{g}$. The exponential map, $\exp : \mathbb{R}^{\dim\mathfrak{g}} \to \mathcal{G}$, is defined as: $\exp(\boldsymbol{\xi}) = \mathrm{expm}(\boldsymbol{\xi}^\wedge)$, where expm is the usual exponential of $N \times N$ matrices. The inverse operator of $(\cdot)^\wedge$ is denoted as $(\cdot)^\vee : \mathfrak{g} \to \mathbb{R}^{\dim\mathfrak{g}}$. The adjoint matrix of any vector $\boldsymbol{\xi} \in \mathbb{R}^{\dim\mathfrak{g}}$ at $\mathbf{X} \in \mathcal{G}$ is defined as $\mathbf{Ad}_X\boldsymbol{\xi} = (\mathbf{X}\boldsymbol{\xi}^\wedge\mathbf{X}^{-1})^\vee$.

3. PROBLEM FORMULATION

3.1 Hybrid Systems with State-Triggered Jumps on Matrix Lie Groups

This study considers the following deterministic, nonlinear hybrid dynamical system on the matrix Lie group $\mathcal{G}$:

$$\begin{cases} \frac{d}{dt}\mathbf{X}_t = \mathbf{f}_{u_t}(\mathbf{X}_t), & \text{if } \mathbf{X}_t \in D\backslash S; \\ \mathbf{X}_{t^+} = \boldsymbol{\Delta}(\mathbf{X}_t), & \text{if } \mathbf{X}_t \in S, \end{cases} \tag{1}$$

where $\mathbf{X}_t \in \mathcal{G}$ is the state, $\mathbf{u}_t \in \mathbb{R}^p$ is the input, and $\boldsymbol{\Delta}(\mathbf{X}_t) : \mathcal{G} \to \mathcal{G}$ is the jump map. $\mathbf{f}_{u_t}(\mathbf{X}_t) : \mathcal{G} \to T_X\mathcal{M}$ is the vector field of the continuous-time subsystem, where $T_X\mathcal{M}$ is the tangent space at $\mathbf{X}$ with $\mathcal{M}$ the Lie group's manifold. The variable $\mathbf{X}_{t^+}$ represents the value of $\mathbf{X}$ just after the jump at t. The domain D is a closed subset of $\mathcal{G}$. The guard S is a co-dimension one submanifold of D. The domain and guard are defined as:

$$D := \{\mathbf{X} \in \mathcal{G} \ : \ \phi(t, \mathbf{X}) \geq 0\} \text{ and} \tag{2}$$

$$S := \{\mathbf{X} \in \mathcal{G} \ : \ \phi(t, \mathbf{X}) = 0 \text{ and } \dot{\phi}(t, \mathbf{X}) < 0\}. \tag{3}$$

Note that the state dependence of the scalar function $\phi : \mathbb{R}^+ \times \mathcal{G} \to \mathbb{R}$ causes the jump to be state-triggered.

Assumption 1. *This study considers the following assumptions on the system model:*

(A1) The vector field $\mathbf{f}_{u_t}$, the jump map $\boldsymbol{\Delta}$, and the function ϕ are locally Lipschitz in their arguments.
(A2) No state trajectories undergo infinite jumps within a finite period (i.e., Zeno behavior is excluded).
(A3) The continuous-time subsystem is group affine as defined next.

3.2 Group Affine Continuous-Time Subsystem

As this study focuses on filter design for hybrid systems with group affine continuous-time subsystems, this subsection explains the definition and property of group affine systems (Barrau and Bonnabel (2017)).

Definition 2. *(Group affine condition) A continuous-time system $\frac{d}{dt}\mathbf{X}_t = \mathbf{f}_{u_t}(\mathbf{X}_t)$ on a matrix Lie group $\mathcal{G}$ is group affine if $\mathbf{f}_{u_t}$ satisfies $\mathbf{f}_{u_t}(\mathbf{ab}) = \mathbf{f}_{u_t}(\mathbf{a})\mathbf{b} + \mathbf{a}\mathbf{f}_{u_t}(\mathbf{b}) - \mathbf{a}\mathbf{f}_{u_t}(\mathbf{I}_N)\mathbf{b}$ for all $t \in \mathbb{R}^+$, where $\mathbf{a}, \mathbf{b} \in \mathcal{G}$.*

Definition 3. *(Invariant estimation errors on Lie groups) Let $\bar{\mathbf{X}}_t \in \mathcal{G}$ be the state estimate. Then the left- and right-invariant estimation errors of the system $\frac{d}{dt}\mathbf{X}_t = \mathbf{f}_{u_t}(\mathbf{X}_t)$ are respectively defined as $\boldsymbol{\eta}^l_t := \mathbf{X}_t^{-1}\bar{\mathbf{X}}_t$ and $\boldsymbol{\eta}^r_t := \bar{\mathbf{X}}_t\mathbf{X}_t^{-1}$ with superscripts l (and r) indicating the left (and right) invariance.*

Proposition 4. *(Continuous-time error dynamics independent from state trajectories on Lie groups): Consider a group affine continuous-time system $\frac{d}{dt}\mathbf{X}_t = \mathbf{f}_{u_t}(\mathbf{X}_t)$. The dynamics of the left- and right-invariant errors of the system are independent from the state trajectory $\mathbf{X}_t$; that is, $\frac{d}{dt}\boldsymbol{\eta}^l_t = \mathbf{g}^l_{u_t}(\boldsymbol{\eta}^l_t)$ and $\frac{d}{dt}\boldsymbol{\eta}^r_t = \mathbf{g}^r_{u_t}(\boldsymbol{\eta}^r_t)$ with $\mathbf{g}^l_{u_t} = \mathbf{f}_{u_t}(\boldsymbol{\eta}^l) - \mathbf{f}_{u_t}(\mathbf{I}_N)\boldsymbol{\eta}^l$ and $\mathbf{g}^r_{u_t} = \mathbf{f}_{u_t}(\boldsymbol{\eta}^r) - \boldsymbol{\eta}^r\mathbf{f}_{u_t}(\mathbf{I}_N)$.*

Proposition 5. *(Linear continuous-time dynamics of logarithmic errors): Consider a group affine continuous-time system $\frac{d}{dt}\mathbf{X}_t = \mathbf{f}_{u_t}(\mathbf{X}_t)$. For any initial values of the invariant error $\boldsymbol{\eta}^i_{t_0} \in \mathcal{G}$ with $i \in [l, r]$, let the vector $\boldsymbol{\xi}^i_t \in \mathbb{R}^{dim\mathfrak{g}}$ be defined such that $exp(\boldsymbol{\xi}^i_{t_0}) = \boldsymbol{\eta}^i_{t_0}$ and $\frac{d}{dt}\boldsymbol{\xi}^i_t = \mathbf{A}^i_t\boldsymbol{\xi}^i_t$ for $t > t_0$, where the matrix $\mathbf{A}^i_t$ is defined as $\mathbf{g}^i_{u_t}(exp(\boldsymbol{\xi}^i_t)) =: \mathbf{A}^i_t\boldsymbol{\xi}^i_t + \mathcal{O}(\|\boldsymbol{\xi}^i_t\|^2)$. Then, for any $t > t_0$ and arbitrarily large $\boldsymbol{\eta}^i_t$, the correspondence $\boldsymbol{\eta}^i_t = exp(\boldsymbol{\xi}^i_t)$ always holds.*

By Proposition 5, the equation of the logarithmic error $\boldsymbol{\xi}_t$ for a group affine system $\frac{d}{dt}\mathbf{X}_t = \mathbf{f}_{u_t}(\mathbf{X}_t)$ is exactly linear, which is the key to the provable error convergence of InEKF as a stable observer for deterministic, group affine systems without state-triggered jumps.

3.3 Filter Design for the Continuous-Time Subsystem

The proposed HInEKF directly utilizes the existing InEKF methodology (Barrau and Bonnabel (2017); Barrau and Bonnabel (2018)) to handle the group affine continuous-time subsystem in Eq. (1), as explained next.

For brevity, only the *right-invariant* EKF (RInEKF) algorithm is presented, and the corresponding superscript r is dropped for notational simplicity. The left-invariant counterpart is given in (Barrau and Bonnabel (2017)).

Process and measurement models. The process model of the continuous-time subsystem in Eq. (1) is $\frac{d}{dt}\mathbf{X}_t = \mathbf{f}_{u_t}(\mathbf{X}_t)$. The j^{th} element of a class of measurement models that satisfies the *right-invariant* form (Barrau and Bonnabel (2017)) is $\mathbf{Y}_{j,t_n} = \mathbf{X}_{t_n}^{-1}\mathbf{d}_j,\ j \in \{1, 2, ...k\}$, where t_n ($n \in \mathbb{N}^+$) is the timing of the n^{th} measurement update, k is the number of outputs, $\mathbf{Y}_{j,t_n} \in \mathbb{R}^N$ is the j^{th} output at time step t_n, and $\mathbf{d}_j \in \mathbb{R}^N$ is a known vector.

Filter design for continuous-time subsystems. The propagation and the *right-invariant* measurement update are respectively given by:

$$\begin{aligned} \frac{d}{dt}\bar{\mathbf{X}}_t &= \mathbf{f}_{u_t}(\bar{\mathbf{X}}_t) \text{ (Propagation)} \\ \bar{\mathbf{X}}_{t_n}^{\dagger} &= \exp(\mathbf{L}_{t_n}\mathbf{Z}_{t_n})\bar{\mathbf{X}}_{t_n} \text{ (Update)} \end{aligned} \tag{4}$$

with $\mathbf{Z}_{t_n} := [(\bar{\mathbf{X}}_{t_n}\mathbf{Y}_{1,t_n} - \mathbf{d}_1)^T, \ldots, (\bar{\mathbf{X}}_{t_n}\mathbf{Y}_{k,t_n} - \mathbf{d}_k)]^T$, where $\bar{\mathbf{X}}_{t_n}^{\dagger}$ is the updated state estimate at time step t_n and $\mathbf{L}_{t_n} \in \mathbb{R}^{\dim\mathfrak{g}\times kN}$ is the gain to be designed next.

Gain computation based on a noisy system. To design the filter gain $\mathbf{L}_{t_n}$ for the continuous-time subsystem, we first associate a fictitious noisy system with the process and measurement models (Barrau and Bonnabel (2017); Barrau and Bonnabel (2018); Grizzle and Song (1995)). Design the gain based on a noisy system could help inform the filter tuning for real-world stochastic systems. The noisy system and measurements are expressed as:

$$\frac{d}{dt}\mathbf{X}_t = \mathbf{f}_{u_t}(\mathbf{X}_t) + \mathbf{X}_t\boldsymbol{w}_t \text{ and} \tag{5}$$

$$\mathbf{Y}_{j,t_n} = \mathbf{X}_{t_n}^{-1}(\mathbf{d}_j + \mathbf{V}_{j,t_n}) + \mathbf{B}_{j,t_n}, \tag{6}$$

where $\boldsymbol{w}_t \in \mathfrak{g}$ represents a continuous white noise with covariance matrix $\mathbf{Q}_t$, and the vectors $\mathbf{V}_{j,t_n}$ and $\mathbf{B}_{j,t_n}$ are noises with known characteristics. Accordingly, during the propagation step, the linear error dynamics in $\mathbb{R}^{\dim\mathfrak{g}}$ becomes:

$$\frac{d}{dt}\boldsymbol{\xi}_t = \mathbf{A}_t\boldsymbol{\xi}_t + \bar{\boldsymbol{w}}_t, \tag{7}$$

where the noise $\bar{\boldsymbol{w}}_t = -\mathbf{Ad}_{\bar{X}_t}(\boldsymbol{w}_t^{\vee})$ is zero-mean Gaussian.

During the update step, linearized error equation can be obtained through a first-order Taylor expansion of the update in Eq. (4) with the noise $\mathbf{V}_{j,t_n}$ and $\mathbf{B}_{j,t_n}$ in Eq. (6) incorporated. The resulting linearized error equation is:

$$\boldsymbol{\xi}_{t_n}^{\dagger} = (\mathbf{I} - \mathbf{L}_{t_n}\mathbf{H})\boldsymbol{\xi}_{t_n} + \mathbf{L}_{t_n}(\mathbf{V}_{t_n} + \bar{\mathbf{B}}_{t_n}), \tag{8}$$

where $\mathbf{I}$ is an identity matrix with an appropriate dimension. The matrix $\mathbf{H} \in \mathbb{R}^{kN\times dim\mathfrak{g}}$ and the vectors $\bar{\mathbf{V}}_{t_n} \in \mathbb{R}^{kN}$ and $\mathbf{B}_{t_n} \in \mathbb{R}^{kN}$ are defined as $\mathbf{H}\boldsymbol{\xi} = [((\boldsymbol{\xi})^{\wedge}\mathbf{d}_1)^T, \ldots, ((\boldsymbol{\xi})^{\wedge}\mathbf{d}_k)^T]^T$, $\mathbf{V}_{t_n} = [\mathbf{V}_{1,t_n}^T, \ldots, \mathbf{V}_{k,t_n}^T]^T$, and $\bar{\mathbf{B}}_{t_n} = [\bar{\mathbf{X}}_{t_n}\mathbf{B}_{1,t_n}, \ldots, \bar{\mathbf{X}}_{t_n}\mathbf{B}_{k,t_n}]^T$.

The gain $\mathbf{L}_{t_n}$ is computed through the following Riccati equation of the matrix $\mathbf{P}_t \in \mathbb{R}^{\dim\mathfrak{g}\times\dim\mathfrak{g}}$, which is built upon the linearized error equations in Eqs. (7) and (8):

$$\frac{d}{dt}\mathbf{P}_t = \mathbf{A}_t\mathbf{P}_t + \mathbf{P}_t\mathbf{A}_t^T + \bar{\mathbf{Q}}_t \text{ and } \mathbf{P}_{t_n}^{\dagger} = (\mathbf{I} - \mathbf{L}_{t_n}\mathbf{H})\mathbf{P}_{t_n} \tag{9}$$

with $\mathbf{S}_{t_n} = \mathbf{H}\mathbf{P}_{t_n}\mathbf{H}^T + \bar{\mathbf{N}}_{t_n}$ and $\mathbf{L}_{t_n} = \mathbf{P}_{t_n}\mathbf{H}^T\mathbf{S}_{t_n}^{-1}$. The matrix $\bar{\mathbf{P}}_{t_n}^{\dagger}$ is the updated value of $\mathbf{P}_t$ at time step t_n, and $\bar{\mathbf{Q}}_t$ and $\bar{\mathbf{N}}_{t_n}$ are the covariance matrices of the noise $\bar{\boldsymbol{w}}_t$ and $\mathbf{V}_{t_n} + \bar{\mathbf{B}}_{t_n}$, respectively. The initial value $\mathbf{P}_0$ of the matrix $\mathbf{P}_t$ is set to be symmetric, positive definite, i.e., $\mathbf{P}_0 = \mathbf{P}_0^T$ and $\mathbf{P}_0 > 0$.

Asymptotic error convergence for the continuous-time subsystem. The following proposition provides the sufficient stability conditions of the proposed HInEKF for the continuous-time group affine subsystem, which is a direct adaptation of the existing InEKF theory for systems without state-triggered jumps.

Assumption 6. *Consider the group affine continuous-time subsystem $\frac{d}{dt}\mathbf{X}_t = \mathbf{f}_{u_t}(\mathbf{X}_t)$ and the associated filter design in Eqs. (4) and (9). Let $\boldsymbol{\Phi}_{t_0}^t$ denote the square matrix defined by $\boldsymbol{\Phi}_{t_0}^{t_0} = \mathbf{I}$, $\frac{d}{dt}\boldsymbol{\Phi}_{t_0}^t = \mathbf{A}_t\boldsymbol{\Phi}_{t_0}^t$, and $\boldsymbol{\Phi}_{t_0}^{t^+} = (\mathbf{I} - \mathbf{L}_{t_n}\mathbf{H})\boldsymbol{\Phi}_{t_0}^t$. Assume that there exist positive numbers α_1, α_2, β_1, β_2, δ_1, δ_2, and δ_3 and a positive integer M such that following conditions are satisfied about the system's true state trajectory $\mathbf{X}_t$:*

(B1) $(\boldsymbol{\Phi}_{t_n}^{t_{n+1}})^T\boldsymbol{\Phi}_{t_n}^{t_{n+1}} \geq \delta_1\mathbf{I}$.

(B2) $\exists q \in \mathbb{N}^+,\ \forall t > t_0, \exists\mathbf{G}_t \in \mathbb{R}^{p\times q},\ \bar{\mathbf{Q}}_t = \mathbf{G}_t\tilde{\mathbf{Q}}\mathbf{G}_t^T$, *where* $\tilde{\mathbf{Q}} \geq \delta_2\mathbf{I}$.

(B3) $\bar{\mathbf{N}}_{t_n} \geq \delta_3\mathbf{I}$.

(B4) $\alpha_2\mathbf{I} \geq \int_{t_{n-M}}^{t_n}\boldsymbol{\Phi}_s^{t_n}\bar{\mathbf{Q}}_s(\boldsymbol{\Phi}_s^{t_n})^T ds \geq \alpha_1\mathbf{I}$.

(B5) $\beta_2\mathbf{I} \geq \sum_{i=n-M}^{n-1}(\boldsymbol{\Phi}_{t_{i+1}}^{t_n})^T\mathbf{H}^T\bar{\mathbf{N}}_{t_n}^{-1}\mathbf{H}\boldsymbol{\Phi}_{t_{i+1}}^{t_n} \geq \beta_1\mathbf{I}$.

Note that the conditions in Assumption 6 are analogous to the sufficient conditions (Deyst and Price (1968)) that guarantee a Kalman filter to be a stable observer for linear deterministic systems without state-triggered jumps.

Proposition 7. *(Asymptotic stability of HInEKF for the continuous-time subsystems) Consider the group affine continuous-time subsystem $\frac{d}{dt}\mathbf{X}_t = \mathbf{f}_{u_t}(\mathbf{X}_t)$ and the associated filter design in Eqs. (4) and (9). Suppose the initial value $\mathbf{P}_{t_0}$ is chosen as symmetric, positive-definite. If there exist positive numbers α_1, α_2, β_1, β_2, δ_1, δ_2, and δ_3 and a positive integer M such that the conditions in Assumption 6 are satisfied about the system's true trajectory $\mathbf{X}_t$, then by the existing InEKF theory (Barrau and Bonnabel (2017)), the proposed HInEKF is an asymptotically stable observer for the continuous-time subsystem.*

3.4 Problem Statement

The proposed HInEKF for the continuous-time subsystem has been introduced based on the direct extension of the existing InEKF for group affine systems without state-triggered jumps. The remaining tasks of the proposed filter derivation is: a) to explicitly handle the state-triggered jumps in filter design; b) to provide sufficient stability conditions of the resulting hybrid error system; and c) to completely characterize a class of nonlinear jumps whose

error jump maps are identity on the Matrix Lie groups, thus greatly simplifying the observer designs for systems with such jump maps.

4. FILTERING AT STATE-TRIGGERED JUMPS

This section introduces the proposed filtering algorithm that provides state and covariance estimates on the matrix Lie group across a jump event. The proposed algorithm, in conjunction with the design (Eqs. (4) and (9)) for the continuous-time subsystems, form the complete HInEKF framework.

Assumption 8. *The following assumptions on the jump events are considered in the proposed filter design:*

(C1) The occurrence of jumps is instantaneously detected; that is, the jump times are directly sensed (Hartley et al. (2020)).
(C2) Measurement updates are not available at jumps.
(C3) Without loss of generality, the timings of measurement updates for the continuous-time subsystem do not coincide with the jumps events.

As it is assumed in this study that there is no measurement update at a jump (Assumption 8), the focus of the filter design at a jump event is to propagate the state estimate $\bar{\mathbf{X}}_t$ and covariance estimate $\mathbf{P}_t$ across the jump. Similar to the filtering of the continuous-time subsystem, the proposed propagation for the jump event is synthesized by considering the true state as a random variable, with the objective of closely reflecting the statistic distribution of the true state across a jump event. This will help ensure that the computation of the filter gain in Eq. (9) would minimize the error variance for the linearized, Gaussian continuous-time subsystem in Eqs. (7) and (8).

4.1 HInEKF Algorithm for State-triggered Jumps

The key to the proposed propagation step is to form the linearization of a jump event based on its saltation matrix. Such linearization has been utilized for a filter design in Euclidean space (i.e., SEKF), and the proposed algorithm extends it to matrix Lie groups. This linearization is theoretically more accurate than the one adopted in previous InEKF design for legged locomotion (Hartley et al. (2020)), which is constructed based on the Jacobian matrix of the jump map.

Process model. Under the assumption that the jumps are instantaneously detected (Assumption 8), it is reasonable to let the state and covariance estimates jump simultaneously as the true state jumps. By the hybrid system dynamics in Eq. (1), the process model of a jump at time t is given by $\mathbf{X}_{t^+} = \boldsymbol{\Delta}(\mathbf{X}_t)$.

Jump map linearization. The propagation of the state and covariance estimates is based on the following first-order approximation of the true state at the linearization point $\bar{\mathbf{X}}_t$:

$$\mathbf{X}_{t^+} = \boldsymbol{\Delta}(\bar{\mathbf{X}}_t) + \boldsymbol{\Xi}(\bar{\mathbf{X}}_t)\boldsymbol{\xi}_t + \mathbb{O}(\|\boldsymbol{\xi}_t\|^2), \tag{10}$$

with $\boldsymbol{\Xi}(\bar{\mathbf{X}}_t) := \mathbf{J}(\bar{\mathbf{X}}_t) + ((\mathbf{f}^+_{u_t}(\boldsymbol{\Delta}^{-1}(\bar{\mathbf{X}}_t))^\vee - \mathbf{J}(\bar{\mathbf{X}}_t)(\mathbf{f}^-_{u_t}\bar{\mathbf{X}}_t^{-1})^\vee - \frac{D\boldsymbol{\Delta}}{Dt}(\bar{\mathbf{X}}_t)) \cdot \frac{\frac{D\boldsymbol{\phi}}{D\mathbf{X}}(\bar{\mathbf{X}}_t)}{\frac{D\boldsymbol{\phi}}{D\mathbf{X}}(\bar{\mathbf{X}}_t) + \frac{D\boldsymbol{\phi}}{D\mathbf{X}}(\bar{\mathbf{X}}_t)\mathbf{f}^-_{u_t}}$, where $\mathbf{f}^+_{u_t} = \mathbf{f}_{u_t}(\boldsymbol{\Delta}(\bar{\mathbf{X}}_t))$, $\mathbf{f}^-_{u_t} = \mathbf{f}_{u_t}(\bar{\mathbf{X}}_t)$, and the left Jacobian $\mathbf{J}(\mathbf{X}_t) : \mathfrak{g} \to \mathfrak{g}$ is defined as $\mathbf{J}(\mathbf{X}_t) := \frac{D\boldsymbol{\Delta}}{D\mathbf{X}}(\mathbf{X}_t)$. The expression of the saltation matrix is obtained by extending the usual expression in Euclidean space (Kong et al. (2020)) to matrix Lie groups, by applying the chain rule of differentiation and computing Jacobian matrices on matrix Lie groups.

Propagation through the jump. Analogous to the filter design of the continuous-time subsystem, we consider the logarithmic error $\boldsymbol{\xi}_t$ at the jump time t to be a Gaussian random variable with zero mean and covariance $\mathbf{P}_t$. Then, the proposed propagation of $\bar{\mathbf{X}}_t$ and $\mathbf{P}_t$ is expressed as:

$$\bar{\mathbf{X}}_{t^+} = \boldsymbol{\Delta}(\bar{\mathbf{X}}_t) \text{ and } \mathbf{P}_{t^+} = \boldsymbol{\Xi}(\bar{\mathbf{X}}_t)\mathbf{P}_t\boldsymbol{\Xi}^T(\bar{\mathbf{X}}_t) \tag{11}$$

which accurately reflects the mapping of the mean and covariance of the state across a jump for the linearization at $\bar{\mathbf{X}}_t$ in Eq. (10). For non-Gaussian systems, this algorithm serves as an approximation of the propagation of the essential features of the true state's conditional probability density function at a jump event.

4.2 Summary of HInEKF

The complete algorithm of the proposed Right-HInEKF is summarized in Algorithm 1. The Left-HInEKF is analogous to this algorithm and omitted for brevity.

Algorithm 1 Right-HInEKF for Hybrid Systems with State-Triggered Jumps

Initialize $\bar{\mathbf{X}}_{t_0} \in \mathcal{G}$. Initialize $\mathbf{P}_{t_0} \in \mathbb{R}^{\dim\mathfrak{g}\times\dim\mathfrak{g}}$ as symmetric, positive-definite. Define $\bar{\mathbf{Q}}_t$ and $\bar{\mathbf{N}}_{t_n}$ as covariance matrices of $\bar{\boldsymbol{w}}_t$ and $\mathbf{V}_{t_n} + \bar{\mathbf{B}}_{t_n}$ respectively.
while True **do**
  if a jump is detected **then**
    Propagation at a jump
    $\bar{\mathbf{X}}^\dagger_t = \boldsymbol{\Delta}(\bar{\mathbf{X}}_{t^-}), \quad \mathbf{P}^\dagger_t = \mathbf{J}^\Delta_t\mathbf{P}_{t^-}(\mathbf{J}^\Delta_t)^T + \mathbf{Q}^\Delta_t$
  else
    Propagation for continuous-time subsystem
    $\frac{d}{dt}\bar{\mathbf{X}}_t = \mathbf{f}_{u_t}(\bar{\mathbf{X}}_t), \quad \frac{d}{dt}\mathbf{P}_t = \mathbf{A}_t\mathbf{P}_t + \mathbf{P}_t\mathbf{A}_t^T + \bar{\mathbf{Q}}_t$
    Update for continuous-time subsystem
    $\mathbf{S}_{t_n} = \mathbf{H}\mathbf{P}_{t_n}\mathbf{H}^T + \bar{\mathbf{N}}_{t_n}, \mathbf{L}_{t_n} = \mathbf{P}_{t_n}\mathbf{H}^T\mathbf{S}^{-1}_{t_n}$
    $\mathbf{P}^\dagger_{t_n} = [\mathbf{I} - \mathbf{L}_{t_n}\mathbf{H}]\mathbf{P}_{t_n}, \ \bar{\mathbf{X}}^\dagger_{t_n} = \exp(\mathbf{L}_{t_n}\mathbf{Z}_{t_n})\bar{\mathbf{X}}_{t_n}$
  end
end

5. CONVERGENCE ANALYSIS

This section introduces the convergence analysis of the proposed HInEKF design for deterministic nonlinear hybrid dynamical systems with state-triggered jumps and group affine continuous-time subsystems. The analysis produces a set of sufficient conditions under which the filter is an asymptotically stable observer for the considered deterministic hybrid dynamical system.

Because the jump times are directly sensed (Assumption 8), the state estimate jumps simultaneously with the true state. Thus, intermittent error divergence caused by the mismatch between their jump times (Bernard and Sanfelice (2018)) do not exist, which allows Lyapunov-based stability theory to be exploited to analyze the closed-loop stability of the hybrid filter.

Theorem 9 (Sufficient stability conditions.)**.** *Consider Assumptions 1, 6, and 8. Let τ_m be the m^{th} jump time with $m \in \{0, 1, 2, ...\}$ and $\tau_0 = t_0$. Assume that there exists a positive integer k_τ such that $\tau_{m+1} - \tau_m > k_\tau M \Delta T$, where ΔT is the sampling interval of the measurement update for the continuous-time subsystem and the positive integer M is defined in Assumption 6. Then, the proposed HInEKF in Eqs.* (4)*,* (9)*, and* (11) *is a (locally) asymptotically stable observer for the overall hybrid system in Eq.* (1) *if there exists sufficiently large k_τ or if there exist appropriately chosen $\bar{\mathbf{Q}}_t$ and $\bar{\mathbf{N}}_t$ that guarantee a sufficiently high convergence rate for the continuous-time error dynamics.*

Sketch of proof. The key to the proof of Theorem 9 is the stability analysis of the hybrid closed-loop error system based on the multiple Lyapunov function (MLF) theory (Branicky (1998)). According to the MLF stability theory, a hybrid system is asymptotically stable if there exists a Lyapunov function candidate that asymptotically decreases with each domain and their values right after each switching form a strictly decreasing sequence. Guided by the MLF stability conditions, Theorem 9 can be proved by designing the Lyapunov function candidate as $V_t(\boldsymbol{\xi}_t) = \boldsymbol{\xi}_t^T \mathbf{P}_t^{-1} \boldsymbol{\xi}_t$ and by exploiting the provable error convergence of the continuous-time subsystem (Proposition 7). The full proof is omitted for space consideration. □

6. IDENTITY ERROR JUMP MAP ON LIE GROUPS

This section introduces a set of conditions that characterize a class of hybrid dynamical systems whose error jump maps are identity on the matrix Lie group $\mathcal{G}$, as well as the attractive convergence property of their error systems under the proposed HInEKF.

Theorem 10. *(Identity error jump map on matrix Lie groups) Consider the jump map $\mathbf{X}_{t^+} = \boldsymbol{\Delta}(\mathbf{X}_t)$. The jump maps of the right- and left-invariant (logarithmic) errors are respectively identity, if and only if for any $t \in \mathbb{R}^+$ and $\mathbf{a}, \mathbf{b} \in \mathcal{G}$ the following conditions respectively hold:*

$$\begin{aligned} &\boldsymbol{\Delta}(\mathbf{ab}) = \mathbf{a}\boldsymbol{\Delta}(\mathbf{b}) \ (\textit{right-invariant}); \\ &\boldsymbol{\Delta}(\mathbf{ab}) = \boldsymbol{\Delta}(\mathbf{a})\mathbf{b} \ (\textit{left-invariant}). \end{aligned} \tag{12}$$

Proof. This proof focuses on the right-invariant case and the superscript r is dropped for brevity. The proof for the left-invariant error can be derived analogously.

Combining $\bar{\mathbf{X}}_t = \boldsymbol{\eta}_t \mathbf{X}_t$, $\bar{\mathbf{X}}_{t^+} = \boldsymbol{\Delta}(\bar{\mathbf{X}}_t)$, and $\mathbf{X}_{t^+} = \boldsymbol{\Delta}(\mathbf{X}_t)$ yields

$$\boldsymbol{\eta}_{t^+} = \boldsymbol{\Delta}_\eta(\boldsymbol{\eta}_t) := \boldsymbol{\Delta}(\boldsymbol{\eta}_t \mathbf{X}_t)(\boldsymbol{\Delta}(\mathbf{X}_t))^{-1}. \tag{13}$$

Equation (13) has to hold for any $\mathbf{X}_t$ and $\boldsymbol{\eta}_t$. Thus, choosing $\mathbf{X}_t = \mathbf{I}_N$, the equation becomes

$$\boldsymbol{\Delta}_\eta(\boldsymbol{\eta}_t) = \boldsymbol{\Delta}(\boldsymbol{\eta}_t)(\boldsymbol{\Delta}(\mathbf{I}_N))^{-1}. \tag{14}$$

Substituting Eq. (14) into Eq. (13) gives

$$\boldsymbol{\Delta}(\boldsymbol{\eta}_t \mathbf{X}_t) = \boldsymbol{\Delta}(\boldsymbol{\eta}_t)(\boldsymbol{\Delta}(\mathbf{I}_N))^{-1}\boldsymbol{\Delta}(\mathbf{X}_t). \tag{15}$$

From Eq. (13), we know that to obtain $\boldsymbol{\Delta}_\eta(\boldsymbol{\eta}_t) = \boldsymbol{\eta}_t$ the following equation needs to hold

$$\boldsymbol{\Delta}(\boldsymbol{\eta}_t) = \boldsymbol{\eta}_t \boldsymbol{\Delta}(\mathbf{I}_N), \tag{16}$$

which, combined with Eq. (15), leads to

$$\boldsymbol{\Delta}(\boldsymbol{\eta}_t \mathbf{X}_t) = \boldsymbol{\eta}_t \boldsymbol{\Delta}(\mathbf{X}_t). \tag{17}$$

□

A real-world estimation problem that involves an identity error jump map on the matrix Lie group is formulated and simulated in Section 7.

Corollary 11. *(Jump map Jacobian): If the jump map $\boldsymbol{\Delta}$ satisfies the identity error jump condition in Eq.* (12)*, Its Jacobian matrix $\mathbf{J}(\mathbf{X}_t) = \frac{D\boldsymbol{\Delta}}{D\mathbf{X}}(\mathbf{X}_t)$ is always exactly identity for any arbitrary estimation error $\boldsymbol{\xi}_t$.*

The proof of Corollary 11 is omitted for brevity.

Proposition 12. *(Simplified filter design and sufficient stability conditions) For a deterministic hybrid dynamical system with form* (1)*, the saltation matrix in the covariance propagation in Eq.* (11) *can be replaced with the Jacobian matrix $\mathbf{J}(\mathbf{X}_t)$. Then, the proposed HInEKF design is an asymptotically stable observer for a hybrid system with identity error jump maps, if the stability conditions for the continuous-time subsystem alone (i.e., the conditions in Assumption 6) are met.*

Proposition 12 is valid essentially because the deterministic hybrid error system becomes a system without state-triggered jumps under the proposed identity error jump condition. The proof is omitted for brevity.

7. CASE STUDY: BIPEDAL WALKING ON A DYNAMIC RIGID SURFACE

This section presents simulation results that validate the stability and convergence performance of the proposed HInEKF through simulations of planar bipedal robot walking on a rigid surface with a vertical motion (e.g., an elevator). Comparative simulations of the SEKF are also presented to illustrate the enhanced performance of the proposed HInEKF.

Note that in this case study some details of the filter design for the continuous-time subsystem (e.g., state representation and process and measurement models) are analogous to previous work (Hartley et al. (2020)). The main differences from the previous design lies in the treatment of the jump event, including the process model of the jump map and accordingly the propagation step at the jump event. Also, the surface is nonstationary instead of static, thus resulting in a time-varying rather than time-invariant guard G, which allows us to validate the proposed theoretical method under a more general form of hybrid transitions.

7.1 Simulation Setup

This subsection explains the simulation setup for the validation of HInEKF and SEKF.

Walking robot. The simulated planar robot has six revolute joints (Fig. 1 a). The walking robot is a single-domain hybrid dynamical system (Gao and Gu (2019)). The average walking speed is 0.35 m/s. The length and height of one walking step are 0.8 m and 0.17 m, respectively. The duration of this simulation is 80 s.

Dynamic rigid surface. A rigid surface (Fig. 1 b), with vertical displacement $y_s = 0.3\cos(2t)$ m, is simulated to emulate common real-world platforms such as elevators.

Sensors. Sensors commonly installed on legged robots are simulated, including: a) an inertial measurement unit (IMU) that measures the linear acceleration and angular velocity of the base frame with respect to (w.r.t.) the base frame; b) encoders that measure the joint angles $\tilde{\mathbf{q}}_t := [q_1, \dots, q_6]^T$; c) LiDAR that measures the relative distance between the robot and known landmarks in the world frame; and d) a contact sensor that detects the occurrence of jump events.

In addition, we assume the surface velocity at the support-foot location is directly measured, which would be realistic for real-world application of legged robot locomotion on moving platforms such as ships whose motion monitoring system measures the surface motion. All sensors return data at 500 Hz except for the LiDAR that runs at 5 Hz.

To assess the filters' performance in a relatively realistic scenario, sensor noises are simulated. To reflect the typical noise characteristics of real-world sensors on legged robots, the sensors' noise standard deviations are: 0.2 m/s^2 (base linear acceleration), 0.04 rad/s (base angular velocity), 1.0° (joint angle), 0.1 m (LiDAR), and 0.1 m/s (surface velocity).

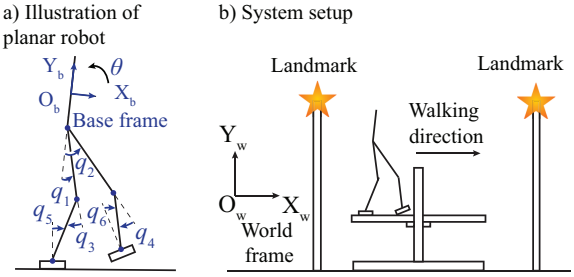

Fig. 1. An illustration of the simulated planar bipedal walking on a dynamic rigid surface.

State representation. The variables to be estimated are chosen as those commonly used in the planning and control of legged locomotion: base position $\mathbf{p}_t = [p_x, p_y]^T$, base velocity $\mathbf{v}_t = [v_x, v_y]^T$, base orientation θ, and support-foot position $\mathbf{d}_t = [d_x, d_y]^T$, which are all expressed in the world frame.

The state representations in HInEKF and SEKF are:

$$\mathbf{X}_t := \begin{bmatrix} \mathbf{R}_t(\theta) & \mathbf{v}_t & \mathbf{p}_t & \mathbf{d}_t \\ \mathbf{0}_{1\times 2} & 1 & 0 & 0 \\ \mathbf{0}_{1\times 2} & 0 & 1 & 0 \\ \mathbf{0}_{1\times 2} & 0 & 0 & 1 \end{bmatrix} \in SE_3(2) \text{ (HInEKF)} \tag{18}$$
$$\mathbf{x}_t = [\mathbf{p}_t^T, \mathbf{v}_t^T, \mathbf{d}_t^T, \theta_t]^T \in \mathbb{R}^7 \text{ (SEKF)}$$

where $\mathbf{R}_t(\theta_t) := \begin{bmatrix} \cos(\theta_t) & -\sin(\theta_t) \\ \sin(\theta_t) & \cos(\theta_t) \end{bmatrix}$ is a rotation matrix.

Covariance matrices. The matrices $\bar{\mathbf{Q}}_t$ and $\bar{\mathbf{N}}_t$ are set to represent the true uncertainty of the process and measurement noises.

Initial errors. Initial base-position errors are 0.33 m (X_w-direction) and 0.7m (Y_w-direction); initial base velocity errors are uniformly distributed within [1, 0.5] m/s (X_w-direction) and [1.3, 1.3] m/s (Y_w-direction); and initial orientation errors are uniformly distributed within [1.3, 1.3] rad. These relatively large initial estimation errors allow us to assess the regions of attraction of HInEKF and SEKF.

7.2 HInEKF Design for Continuous-time Subsystems

Associated noisy system. The input $\mathbf{u}_t$ is defined as $\mathbf{u}_t := [\tilde{\omega}_t, \tilde{\mathbf{a}}_t^T, (\tilde{\mathbf{v}}_t^d)^T]^T$, where the scalar variable $\tilde{\omega}_t$ and the vector $\tilde{\mathbf{a}}_t \in \mathbb{R}^2$ are the raw data returned by the IMU's gyroscope and accelerometer, respectively, and $\tilde{\mathbf{v}}_t^d \in \mathbb{R}^2$ is the sensed surface velocity at the support-foot location.

The continuous-time process model augmented with noise is expressed as:

$$\begin{aligned} \frac{d}{dt}\mathbf{X}_t &= \begin{bmatrix} \mathbf{R}_t(\tilde{\omega}_t)_\times & \mathbf{R}_t\tilde{\mathbf{a}}_t + \mathbf{g} & \mathbf{v}_t & \tilde{\mathbf{v}}_t^d \\ \mathbf{0}_{1\times 2} & 0 & 0 & 0 \\ \mathbf{0}_{1\times 2} & 0 & 0 & 0 \\ \mathbf{0}_{1\times 2} & 0 & 0 & 0 \end{bmatrix} + \mathbf{X}_t\boldsymbol{w}_t, \\ &= \mathbf{f}_{u_t}(\mathbf{X}_t) + \mathbf{X}_t\boldsymbol{w}_t \end{aligned} \tag{19}$$

with $\boldsymbol{w}_t := ([w_t^g, (\boldsymbol{w}_t^a)^T, \mathbf{0}_{1\times 2}, (\boldsymbol{w}_t^d)^T]^T)^\wedge$, where w_t^g, $\boldsymbol{w}_t^a$, and $\boldsymbol{w}_t^d$ are continuous Gaussian white noises of the gyroscope, accelerometer, and contact-velocity measurement, respectively, and $\mathbf{g}$ is the gravitational acceleration.

Note that $\mathbf{f}_{u_t}(\mathbf{X}_t)$ satisfies the group affine condition in Definition 2 (Hartley et al. (2020)). Thus, from Proposition 5, the matrix $\mathbf{A}_t$ in the linear error dynamics during a propagation step can be obtained as:

$$\mathbf{A}_t = \begin{bmatrix} \mathbf{0}_{2\times 2} & \mathbf{0}_{2\times 2} & \mathbf{0}_{2\times 2} & \mathbf{0}_{2\times 2} \\ (\mathbf{g})_\times & \mathbf{0}_{2\times 2} & \mathbf{0}_{2\times 2} & \mathbf{0}_{2\times 2} \\ \mathbf{0}_{2\times 2} & \mathbf{I}_{2\times 2} & \mathbf{0}_{2\times 2} & \mathbf{0}_{2\times 2} \\ (\tilde{\mathbf{v}}_t^d)_\times & \mathbf{0}_{2\times 2} & \mathbf{0}_{2\times 2} & \mathbf{0}_{2\times 2} \end{bmatrix} \tag{20}$$

Measurement model. The measurement includes the leg odometry and the landmark positions relative to the robot. The first right-invariant measurement for the continuous-time subsystem is chosen as the support-foot position relative to the base w.r.t the base frame as computed through the encoder measurement:

$$\underbrace{\begin{bmatrix} \mathbf{h}_p(\tilde{\mathbf{q}}_t) \\ 0 \\ 1 \\ -1 \end{bmatrix}}_{\mathbf{Y}_{1,t}} = \mathbf{X}_t^{-1} \underbrace{\begin{bmatrix} \mathbf{0}_{2\times 1} \\ 0 \\ 1 \\ -1 \end{bmatrix}}_{\mathbf{d}_1} + \underbrace{\begin{bmatrix} \mathbf{J}_p(\tilde{\mathbf{q}}_t)\boldsymbol{w}_t^q \\ 0 \\ 0 \\ 0 \end{bmatrix}}_{\mathbf{B}_{1,t}} \tag{21}$$

where $\boldsymbol{w}_t^q$ is a continuous white noise in encoder raw data, $\tilde{\mathbf{q}}_t \in \mathbb{R}^6$ is the joint angle data returned by encoders, $\mathbf{h}_p$ is the support-foot position relative to the base w.r.t. the base frame, and $\mathbf{J}_p(\tilde{\mathbf{q}}_t) := \frac{\partial \mathbf{h}_p}{\partial \tilde{\mathbf{q}}_t}(\tilde{\mathbf{q}}_t)$ is the contact-point Jacobian matrix.

The second right-invariant measurement for the continuous-time subsystem is chosen as the position of the two known landmarks relative to the robot's base:

$$\underbrace{\begin{bmatrix} \tilde{\mathbf{y}}_{j-1,t}^{\text{LiD}} \\ 0 \\ 1 \\ 0 \end{bmatrix}}_{\mathbf{Y}_{j,t}} = \mathbf{X}_t^{-1} \underbrace{\begin{bmatrix} \mathbf{P}_{j-1,t}^{\text{LM}} \\ 0 \\ 1 \\ 0 \end{bmatrix}}_{\mathbf{d}_j} + \underbrace{\begin{bmatrix} \boldsymbol{w}_{j-1,t}^{\text{LiD}} \\ 0 \\ 0 \\ 0 \end{bmatrix}}_{\mathbf{B}_{j,t}} \tag{22}$$

where $j \in \{2, 3\}$, $\tilde{\mathbf{y}}_{j-1,t}^{\text{LiD}} \in \mathbb{R}^2$ is the raw data returned by the LiDAR, $\mathbf{P}_{j-1,t}^{\text{LM}} \in \mathbb{R}^2$ is the known $(j-1)^{th}$ landmark

position w.r.t the world frame, and $\boldsymbol{w}_{j-1,t}^{\text{LiD}} \in \mathbb{R}^2$ is the continuous Gaussian white noise of the LiDAR data.

Observability. Under the proposed formulation, it can be obtained based on the evaluation method in (Barrau and Bonnabel (2017)) that the continuous-time subsystem is fully observable and fully controllable. That is, the conditions in Assumption 6 are met. The derivation is omitted for brevity.

7.3 HInEKF Design for State-triggered Jumps

Process model. The process model of the jump map is:

$$\mathbf{X}_{t^+} = \begin{bmatrix} \mathbf{R}_t & \mathbf{v}_t & \mathbf{p}_t & \mathbf{d}_t + \mathbf{R}_t \mathbf{h}_d(\tilde{\mathbf{q}}_t) \\ \mathbf{0}_{1\times 2} & 1 & 0 & 0 \\ \mathbf{0}_{1\times 2} & 0 & 1 & 0 \\ \mathbf{0}_{1\times 2} & 0 & 0 & 1 \end{bmatrix} \exp(\boldsymbol{w}_t^{\Delta}), \qquad (23)$$

where $\boldsymbol{w}_t^{\Delta} \in \mathbb{R}^{\dim \mathfrak{g}}$ is the noise vector induced by the encoder noise. The joint angle data $\tilde{\mathbf{q}}_t$ returned by encoders serves as the input to the jump map. The variable $\mathbf{h}_d$ is the new support-foot position just after a jump relative to the previous support-foot position w.r.t. the base frame. Note that the only variable that jumps at a foot touchdown is the support-foot location due to foot switching.

Propagation across a jump event. The jump map $\boldsymbol{\Delta}$ in Eq. (23) satisfies the identity jump map condition for right-invariant errors in Theorem 10. Thus, the logarithmic error $\boldsymbol{\xi}_t$ does not jump at a foot touchdown event; that is, $\boldsymbol{\xi}_{t^+} = \boldsymbol{\xi}_t$ exactly holds. Thus, the Jacobian matrix $\mathbf{J}(\mathbf{X})$, which is used to form the saltation matrix $\boldsymbol{\Xi}(\mathbf{X})$ for the propagation of the matrix $\mathbf{P}_t$ through the jump, is identity. This greatly simplifies the computation of the saltation matrix. In fact, as the rank one update of the saltation matrix is significantly smaller than the Jacobian matrix in our case study, we choose to use the Jacobian to propagate the jump map instead of the full expression of the saltation matrix. This also helps to assess the robustness of the proposed filter design.

7.4 Salted Extended Kalman Filter (SEKF) Design

To compare the performance of the proposed HInEKF with the state-of-the-art filter design for hybrid dynamical systems, the SEKF Kong et al. (2020) is formulated and simulated for the system setup in Section 7.1 under the assumptions of instantaneously detected jumps and no measurement updates at jumps.

Process and measurement models. The SEKF handles the continuous-time subsystem exactly the same as the conventional EKF. The process model of the continuous-time subsystem is : $\frac{d}{dt}\mathbf{p}_t = \mathbf{v}_t$, $\frac{d}{dt}\mathbf{v}_t = \mathbf{R}_t(\tilde{\mathbf{a}}_t + \boldsymbol{w}_t^a) + \mathbf{g}$, $\frac{d}{dt}\mathbf{d}_t = \tilde{\mathbf{v}}_t^d + \boldsymbol{w}_t^d$, and $\frac{d}{dt}\theta_t = \tilde{\omega}_t + w_t^g$.

The measurements for the continuous-time subsystem are: a) the support-foot location w.r.t the base $\mathbf{h}_p(\tilde{\mathbf{q}}_t) = \mathbf{R}_t^T(\theta_t)(\mathbf{d}_t - \mathbf{p}_t) + \mathbf{J}_p(\tilde{\mathbf{q}}_t)\boldsymbol{w}_t^q$ and b) the relative position between robot and the two known landmarks $\tilde{\mathbf{y}}_{j,t}^{\text{LiD}} = \mathbf{R}_t^T(\theta_t)(\mathbf{P}_{j,t}^{LM} - \mathbf{p}_t) + \boldsymbol{w}_{j,t}^{\text{LiD}}$ with $j \in \{1, 2\}$.

At jumps, the SEKF propagates the state estimate based on the process model: $\mathbf{p}_{t^+} = \mathbf{p}_t$, $\mathbf{v}_{t^+} = \mathbf{v}_t$, $\mathbf{d}_{t^+} = \mathbf{d}_t + \mathbf{R}(\theta_t)\mathbf{h}_d(\tilde{\mathbf{q}}_t - \boldsymbol{w}_t^q)$ and $\theta_{t^+} = \theta_t$. At each jump, the solution

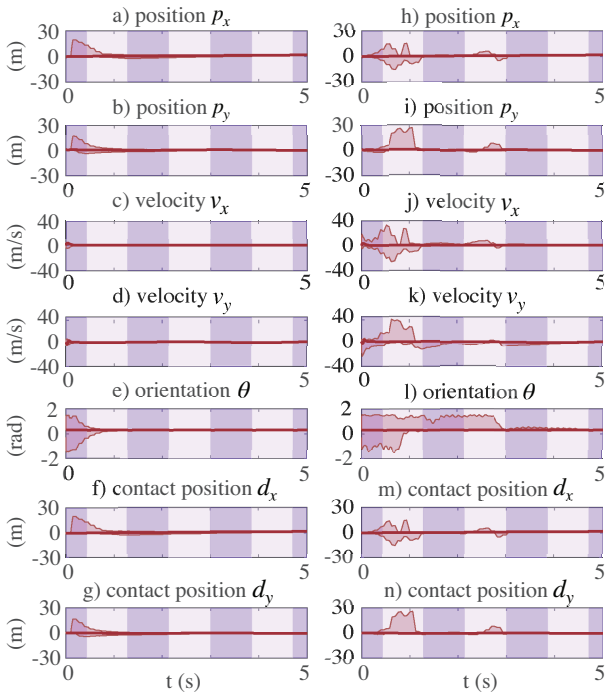

Fig. 2. Results of 63 simulation trials with bipedal robot walking on the vertically moving surface under HInEKF and SEKF. The shaded area includes simulation results of 63 tests. The solid red line represents the group truth. The *jump times* are indicated by the edges of different background colors. Subplots a) - g) are the HInEKF estimation results of the biped's base position $\mathbf{p}_t = [p_x, p_y]^T$, base velocity $\mathbf{v}_t = [v_x, v_y]^T$, orientation θ_t, and the biped's contact foot position $\mathbf{d}_t = [d_x, d_y]^T$. Subplots h) - n) are the corresponding SEKF estimation results.

to the associated Riccaiti equation, $\mathbf{P}_t^{SEKF} \in \mathbb{R}^{7\times 7}$, is propagated through $(\mathbf{P}_t^{SEKF})^{\dagger} = \mathbf{S}\mathbf{P}_t^{SEKF}\mathbf{S}^T$, where $\mathbf{S} : \mathbb{R}^{7\times 7} \to \mathbb{R}^{7\times 7}$ is the saltation matrix expressed in Euclidean space. In contrast to HInKEF, the estimation error of $\mathbf{d}_t$ in Euclidean space is not continuous across a jump event. Thus, the error may suddenly expand just after the jump, and the Jacobian matrix associated with $\mathbf{S}$ will generally be nonidentity.

7.5 Simulation Results

In total, 100 trials are simulated under each of HInEKF and SEKF. The HInEKF converges during all 100 trials whereas the SEKF diverges for 37 trials. Figure 2 displays the 63 successful trials of the SEKF and the corresponding HInEKF results. Figure 3 shows the error norm and Lyapunov function under the HInEKF during one trial.

Validation of identity error jump map condition. As the jump map $\boldsymbol{\Delta}$ in Eq. (23) meets the identity jump map condition in Theorem 10. Thus, as shown in Fig. 3, the logarithmic error $\boldsymbol{\xi}_t$ shows negligible discontinuity at each jump event, which are only induced by sensor noise.

Validation of sufficient stability conditions. The sufficient stability conditions in Theorem 9 are met for the overall hybrid error system, because the walking step duration (i.e., 2.3 s), which is the time interval between two consecutive jumps, is significantly larger than the

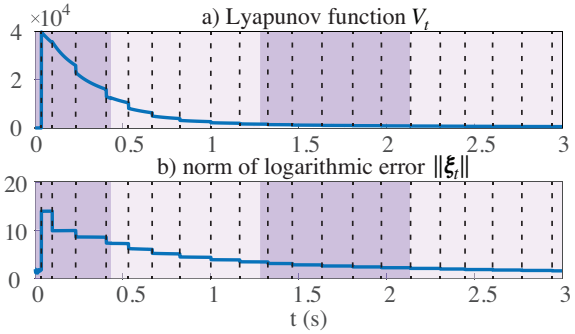

Fig. 3. One trial of bipedal robot walking on the vertically moving surface under HInEKF: a) Lyapunov function and b) norm of logarithmic error $\|\boldsymbol{\xi}_t\|$. The *jump times* are indicated by the edges of different background colors. The black dashed lines highlight the timings when the LiDAR reading is used to update the estimates. Initial base-position errors are 0.33 m (X_w-direction) and 0.7m (Y_w-direction); initial base velocity errors are 1 m/s (X_w-direction) and 1.3 (Y_w-direction); and initial orientation error is -1.3 rad.

filter's sampling period (i.e., 2 ms). This theoretical result is supported by the evolution of the Lyapunov function $V_t = \boldsymbol{\xi}_t^T \mathbf{P}_t^{-1} \boldsymbol{\xi}_t$ in Fig. 3, as well as by the convergence of the logarithmic errors in the subplots a)-g) in Fig. 2.

Error convergence comparison of HInEKF and SEKF. As explained earlier, among the 100 simulation trials, SEKF diverges for 37 trials while HInEKF converges for all trials. During the 63 successful trials as shown in Fig. 2, the proposed HInEKF outperforms the SEKF in terms of convergence rate. Despite the relatively large initial estimation errors, the HInEKF drives the estimation error to rapidly convergence to a small number within 0.8 s. In contrast, it takes roughly 3.5 s for the errors to converge to a similar value under the SEKF.

The differences in error convergence rate are due to: a) for the continuous subsystem, the SEKF is synthesized based on inaccurate linearizations of the process and measurement models, whereas the HInEKF is built upon an exactly linear error equation during the propagation step and b) for the state-triggered jump, the error under the SEKF suddenly expands while the logarithmic error under the HInEKF barely changes.

8. CONCLUSION

This paper has introduced an HInEKF method for a class of hybrid dynamical systems with state-triggered jumps and group affine continuous-time subsystems under the assumption that the jumps are instantaneously detected. Sufficient conditions were provided to guide the design of the HInEKF to ensure the asymptotic convergence of the hybrid error system. Also, a particular class of hybrid dynamical systems whose error jump map under the proposed HInEKF is exactly identity was completely characterized. To validate the performance of the proposed HInEKF, simulations on a bipedal robot walking over nonstationary surfaces were performed. Simulation results demonstrated that the HInEKF achieves significantly higher convergence rate compared with existing SEKF for hybrid dynamical systems with state-triggered jumps.

REFERENCES

Barrau, A. and Bonnabel, S. (2017). The invariant extended kalman filter as a stable observer. IEEE T AUTOMAT CONTR, 62(4), 1797–1812.

Barrau, A. and Bonnabel, S. (2018). Invariant kalman filtering. ANNU REV CONTR, ROB, AUTOM SYST, 1, 237–257.

Bernard, P. and Sanfelice, R.G. (2018). Observers for hybrid dynamical systems with linear maps and known jump times. In PROC IEEE CONF DEC CONTR, 3140–3145.

Bledt, G., Powell, M.J., Katz, B., Di Carlo, J., Wensing, P.M., and Kim, S. (2018). MIT cheetah 3: Design and control of a robust, dynamic quadruped robot. In PROC IEEE/RSJ INT CONF INTEL ROB SYST, 2245–2252.

Bloesch, M., Hutter, M., Hoepflinger, M.A., Leutenegger, S., Gehring, C., Remy, C.D., and Siegwart, R. (2013). State estimation for legged robots-consistent fusion of leg kinematics and imu. ROB, 17, 17–24.

Branicky, M.S. (1998). Multiple lyapunov functions and other analysis tools for switched and hybrid systems. IEEE T AUTOMAT CONTR, 43(4), 475–482.

de Ruiter, A.H. and Forbes, J.R. (2017). Continuous-time kalman filtering on the orthogonal group o (n). INT J ROBUST NONLIN, 27(17), 3466–3487.

Deyst, J. and Price, C. (1968). Conditions for asymptotic stability of the discrete minimum-variance linear estimator. IEEE T AUTOMAT CONTR, 13(6), 702–705.

Gao, Y. and Gu, Y. (2019). Global-position tracking control of a fully actuated nao bipedal walking robot. In PROC AMER CONTR CONF, 4596–4601.

Grizzle, J. and Song, Y. (1995). The extended kalman filter as a local asymptotic observer for nonlinear discrete-time systems. JMSEC, 5(1), 59–78.

Hamed, K.A., Ames, A.D., and Gregg, R.D. (2018). Observer-based feedback controllers for exponential stabilization of hybrid periodic orbits: Application to underactuated bipedal walking. In PROC AMER CONTR CONF, 1438–1445.

Hartley, R., Ghaffari, M., Eustice, R.M., and Grizzle, J.W. (2020). Contact-aided invariant extended kalman filtering for robot state estimation. INT J ROB RES, 39(4), 402–430.

Iqbal, A., Gao, Y., and Gu, Y. (2020). Provably stabilizing controllers for quadrupedal robot locomotion on dynamic rigid platforms. IEEE/ASME T MECHATRON, 25(4), 2035–2044.

Iqbal, A., Mao, Z., and Gu, Y. (2021). Modeling, analysis, and control of slip running on dynamic platforms. ASME L DYN SYST CONTR, 1(2).

Kong, N.J., Payne, J.J., Council, G., and Johnson, A.M. (2020). Mapping distributions through hybrid dynamical systems and its application to Kalman filtering. arXiv preprint arXiv:2007.12233.

Ríos, H., Dávila, J., and Teel, A.R. (2020). State estimation for linear hybrid systems with periodic jumps and unknown inputs. INT J ROBUST NONLIN, 30(15), 5966–5988.

Saccon, A., van de Wouw, N., and Nijmeijer, H. (2014). Sensitivity analysis of hybrid systems with state jumps with application to trajectory tracking. In PROC IEEE CONF DEC CONTR, 3065–3070.